Journal of Medicinal Chemistry

ARTICLE

pubs.acs.org/jmc

# Discovery of a Clinical Candidate from the Structurally Unique Dioxa-bicyclo[3.2.1]octane Class of Sodium-Dependent Glucose Cotransporter 2 Inhibitors

Vincent Mascitti,* Tristan S. Maurer, Ralph P. Robinson, Jianwei Bian, Carine M. Boustany-Kari, Thomas Brandt, Benjamin M. Collman, Amit S. Kalgutkar, Michelle K. Klenotic, Michael T. Leininger, André Lowe, Robert J. Maguire, Victoria M. Masterson, Zhuang Miao, Emi Mukaiyama, Jigna D. Patel, John C. Pettersen, Cathy Préville, Brian Samas, Li She, Zhanna Sobol, Claire M. Steppan, Benjamin D. Stevens, Benjamin A. Thuma, Meera Tugnait, Dongxiang Zeng, and Tong Zhu

Groton Laboratories, Pfizer Global Research & Development, Eastern Point Road, Groton, Connecticut 06340, United States

Supporting Information

**ABSTRACT:** Compound **4** (PF-04971729) belongs to a new class of potent and selective sodium-dependent glucose cotransporter 2 inhibitors incorporating a unique dioxa-bicyclo-[3.2.1]octane (bridged ketal) ring system. In this paper we present the design, synthesis, preclinical evaluation, and human dose predictions related to **4**. This compound demonstrated robust urinary glucose excretion in rats and an excellent preclinical safety profile. It is currently in phase 2 clinical trials and is being evaluated for the treatment of type 2 diabetes.

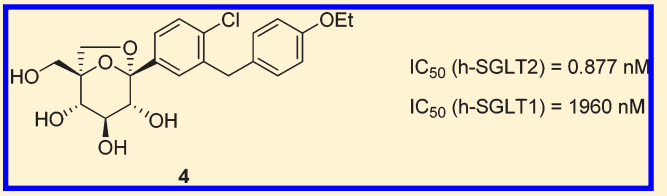


## INTRODUCTION

The alarming and increasing prevalence of type 2 diabetes along with the side effects associated with many current antidiabetic drugs (most notably hypoglycemia and weight gain) has stimulated an intense effort to evaluate new mechanisms to achieve glycemic control.[1,2] Sodium-dependent glucose cotransporter 2 (SGLT2) is a high-capacity, low-affinity transporter expressed selectively in the S1 domain of the proximal tubule in the kidney and is responsible for the reuptake of ~90% of filtered glucose.[3,4] Sodium-dependent glucose cotransporter 1 (SGLT1), on the other hand, is a low-capacity, high-affinity transporter that is found in the kidney, the gut, and other tissues. SGLT1 plays a large role in carbohydrate uptake from the diet.[4,5] Inhibition of SGLT2 induces urinary glucose excretion (UGE) and thereby reduces plasma glucose concentrations.[6,7] This mechanism is the first to address the phenomenon of the increased glucose reabsorption observed in type 2 diabetic patients, which is a key component of the "ominous octet" that characterizes hyperglycemia.[8] Furthermore, since selective SGLT2 inhibition is a glucose-dependent (thereby minimizing the risk of hypoglycemia) and insulin-independent (thus potentially favoring pancreatic $\beta$-cell preservation) mechanism that is associated with weight loss, it has emerged as a very promising approach to the pathophysiologic treatment of type 2 diabetes.[6,7,9,10]

Optimization of the natural product phlorizin (**1**; Figure 1), a nonselective SGLT2 and SGLT1 inhibitor, led to the identification of several selective *O*-aryl glucoside SGLT2 inhibitors;[11,12] however, such inhibitors (e.g., sergliflozin, **2**; Figure 1) were usually associated with degradation by glucosidase enzymes found in the gut and required to be administered as prodrugs.[13] Clinical trials involving compounds from this class were abandoned. The susceptibility to glucosidase degradation was elegantly addressed via the discovery of potent and selective *C*-aryl glucoside SGLT2 inhibitors such as dapagliflozin (**3**; Figure 1).[14] A number of compounds derived from the *C*-aryl glucoside class have been identified and are now at various stages of clinical development.[15−22]

Thus, to date, the SGLT2 inhibitor structural landscape has been dominated by molecules belonging to either one of two classes: *O*-aryl and *C*-aryl glucosides.[15] In both cases, the majority of effort has been spent on modifying the aglycon side chain due to the relative ease of synthesis. However, changes to the aglycon motif are often associated with increased lipophilicity and molecular weight (with resultant implications in terms of pharmacokinetics and/or safety), as well as introduction of structural motifs associated with potential reactive metabolite formation.[23] Additionally, some compounds from the *C*-aryl glucoside class have tested micronucleus positive in vitro.[24]

Herein we report the discovery of **4** (PF-04971729), a compound from a new class of potent and selective SGLT2 inhibitors incorporating a structurally novel dioxa-bicyclo-[3.2.1]octane ring system (Figure 2).[25,26]

**Received:** January 17, 2011
**Published:** March 30, 2011

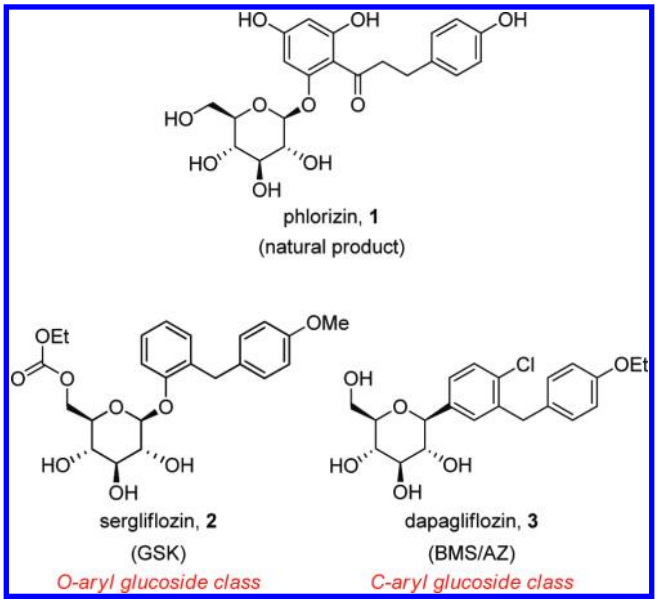


**Figure 1.** From natural product to potent SGLT2 inhibitors.

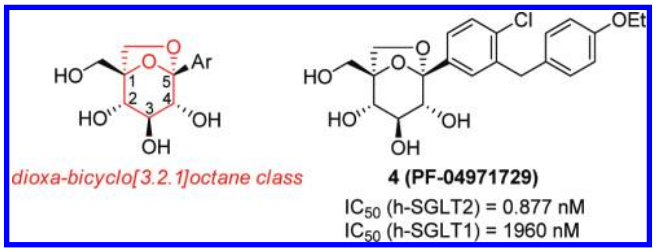


**Figure 2.** Dioxa-bicyclo[3.2.1]octane SGLT2 inhibitors.

## CHEMISTRY

Compounds from this class were prepared in an analogue-friendly fashion starting from advanced intermediate Weinreb amide **5**.[25] Compound **5** was synthesized on multigram scale starting from D-glucose as shown in Scheme 1. Intermediate **6**[27] was oxidized under Swern conditions to the corresponding aldehyde, which, in a one-pot aldol−Cannizzaro[28] sequence, produced intermediate **7** (53% yield over two steps). This two-step protocol allowed for the installation of the tetrasubstituted carbon (C-1) present in the final analogues. Protection of the primary hydroxyl groups in **7** as *p*-methoxybenzyl (PMB) ethers followed by allyl group removal gave lactol intermediate **8** (40% yield over two steps). Oxidation of the lactol to the corresponding lactone **9** and subsequent treatment with *N*,*O*-dimethylhydroxylamine hydrochloride in the presence of trimethylaluminum provided advanced intermediate **5** (42% yield over two steps).[29]

Intermediate **5**, which presents the required carbon framework in the proper oxidation state, was primed for the three-step analoguing sequence as shown in Scheme 2. Nucleophilic addition of the appropriate organolithium reagent to **5** in THF produced the corresponding cyclic lactol **10**. Acid-promoted one-pot PMB removal followed by stereoselective intramolecular trapping of the putative oxonium ion intermediate gave compound **11** containing the desired dioxa-bicyclo[3.2.1]octane ring system.[30] Finally, hydrogenolysis of the benzyl protecting groups under transfer hydrogenation conditions yielded analogues **12**

**Scheme 1. Synthesis of Advanced Intermediate 5**[a]

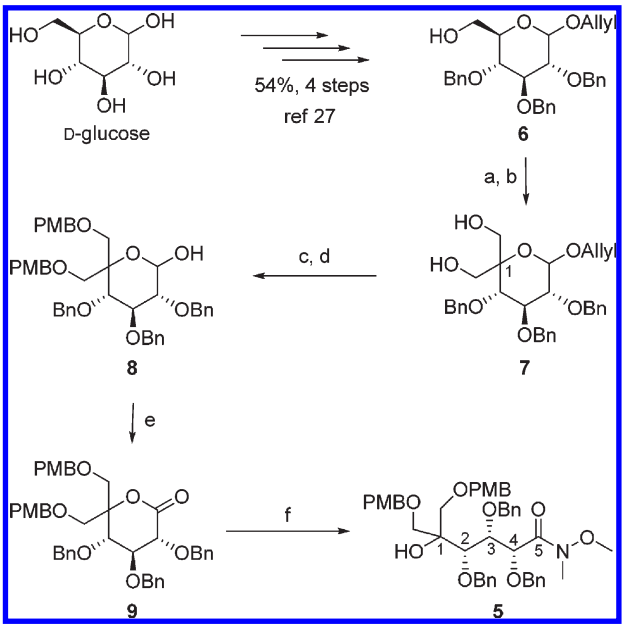


[a] Reagents and conditions: (a) Swern oxidation; (b) NaOH, formaldehyde, *i*-PrOH/water, 23 °C (53%, two steps); (c) PMBBr, NaH, DMF, 0−60 °C (52%); (d) $PdCl_2$, $MeOH/CH_2Cl_2$, 23 °C (78%); (e) Swern oxidation (72%); (f) $AlMe_3$, $MeN(OMe)H_2Cl$, $CH_2Cl_2$, 0−23 °C (58%).

**Scheme 2. Three-Step Analoguing Sequence**[a]

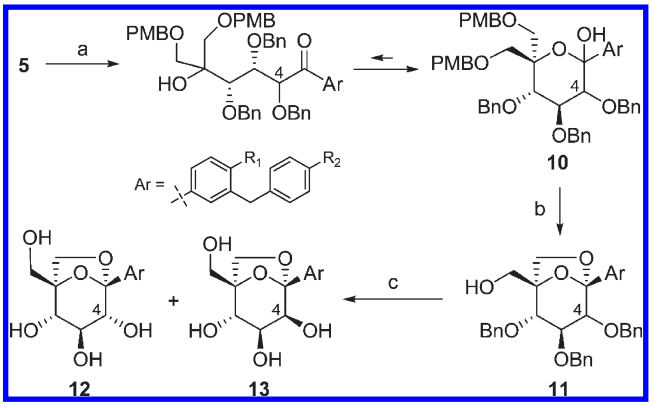


[a] Reagents and conditions: (a) ArLi, THF, −78 to 0−23 °C; (b) TFA, anisole, $CH_2Cl_2$, 23 °C; (c) Pd black, $HCO_2H$, EtOH/THF, 23 °C, then HPLC separation.

and **13** as a mixture of diastereomers at C-4, which were separated by HPLC. The results of single-crystal X-ray diffraction analysis of representative derivatives **14** and **15** are shown in Figures 3 and 4, respectively. The epimerization at C-4 may be rationalized via the formation of a putative enol or enol ether intermediate in the analoguing sequence. Although nonstereoselective, the three-step sequence allowed the rapid exploration of structure−activity relationships. Recently, we reported a stereoselective synthesis providing efficient access to compounds in the class.[31]

## RESULTS AND DISCUSSION

During the course of our program, we developed a pharmacokinetic−pharmacodynamic (PKPD) relationship model to


dx.doi.org/10.1021/jm200049r |*J. Med. Chem.* 2011, 54, 2952–2960

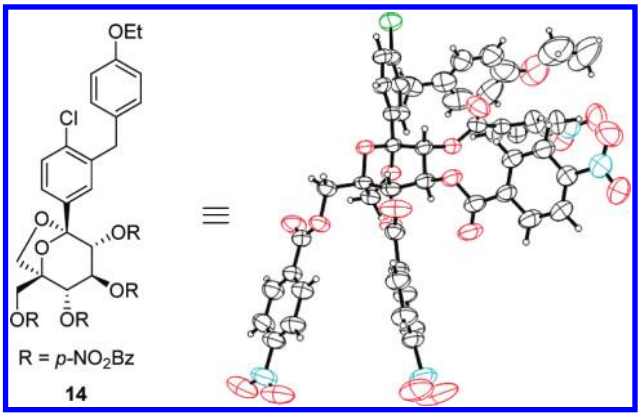


**Figure 3.** ORTEP representation of the X-ray crystal structure of **14**.

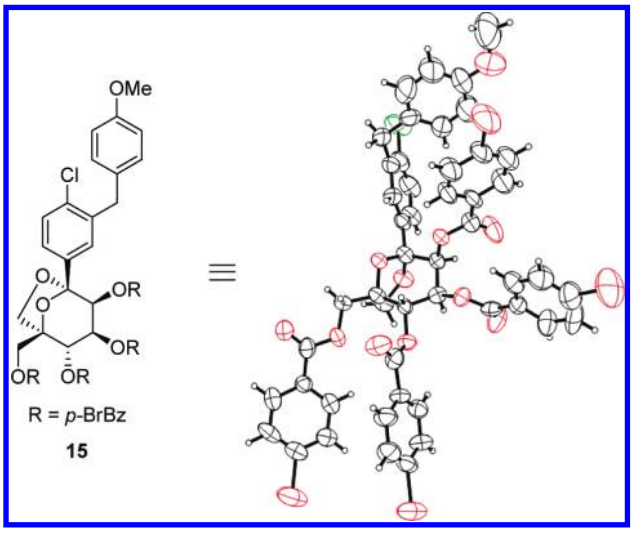


**Figure 4.** ORTEP representation of the X-ray crystal structure of **15**.

help predict a human dosing regimen that would induce near-maximal theoretical UGE at steady state.[32] In this model, human PK predictions were based on allometric scaling from rats after normalization for protein binding differences across species.[33] The PD component was likewise scaled from rats using a differential equation model describing the rate of UGE as a function of inhibitor concentration, inhibitor potency, plasma glucose concentration, glomerular filtration rate, and glucose reuptake.[34]

Previously, we described the synthesis and preclinical evaluation of a series of C-5-spirocyclic *C*-glycoside SGLT2 inhibitors.[35] Unfortunately, in spite of relatively good potency and selectivity for human SGLT2 [$IC_{50}$(h-SGLT2) = 6.98 ± 2.50 nM; $n$ = 8],[36] the lead compound **16** suffered from suboptimal PK (Figure 5).[37] Using rat to human allometry, the predicted total plasma clearance ($CL_{plasma}$) and steady-state volume of distribution ($V_{ss}$) in humans were respectively 4.6 mL/min/kg and 1.9 L/kg. This translated into a short predicted human half-life ($t_{1/2,human}$ < 5.0 h) and a predicted daily efficacious dose of >100 mg to produce near-maximal UGE (60 g/24 h) in healthy volunteers. Furthermore, as we already reported, simulations with the PKPD model also indicated that the predicted dose increases exponentially in relation to decreasing $t_{1/2,human}$.[37]

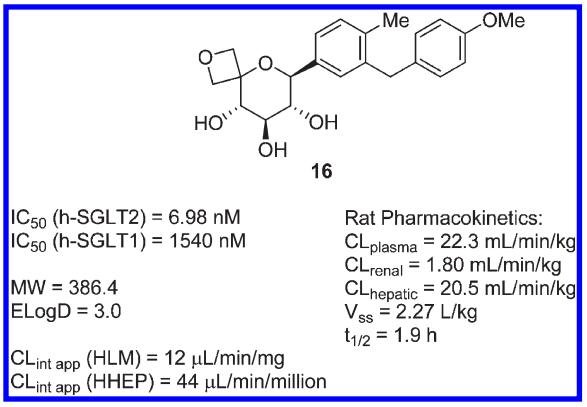


**Figure 5.** Some properties of SGLT2 inhibitor **16**.

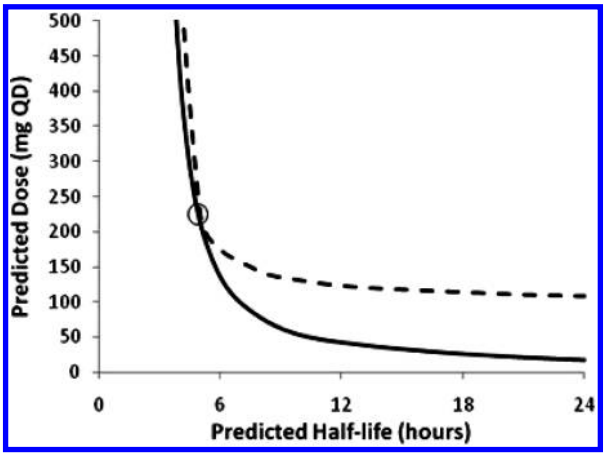


**Figure 6.** Relationship between predicted dose and human half-life for compound **16**. The open symbol represents the predicted human dose (to achieve 60 g of UGE/24 h in healthy volunteers) obtained using the PKPD model assuming a human volume of 1.9 L/kg and a clearance of 4.6 mL/min/kg. The dashed line represents the predicted relationship between dose and $t_{1/2,human}$ obtained via a range of hypothetical volumes between 0.5 and 9.0 L/kg. The solid line represents the predicted relationship between dose and $t_{1/2,human}$ obtained via a range of hypothetical clearances between 1.0 and 10 mL/min/kg.

Given the goal to produce near-maximal UGE in the clinic over 24 h at a daily dose of less than 100 mg, analogues with a longer predicted $t_{1/2,human}$ were desired. Additional PKPD simulations, varying respectively the distribution volume and clearance, were performed to determine the most promising approach for $t_{1/2}$ and dose optimization (Figure 6). These simulations indicated that targeting improvements in predicted clearance was the most viable approach.[38]

Thus, decreasing the projected efficacious dose required increasing $t_{1/2,human}$ via lowering of the predicted clearance in humans. Studies analyzing the elimination mechanism(s) of **16** in rats revealed that $CL_{plasma}$ was largely mediated via hepatic metabolism ($CL_{hepatic}$), the renal clearance ($CL_{renal}$) being generally low and passive (Figure 5).[39] In vitro stability studies on **16** in human hepatic tissue revealed a higher apparent intrinsic clearance ($CL_{int\ app}$)[40,41] in HHEP relative to HLM, suggestive of non-cytochrome P450-mediated metabolic elimination. Indeed, qualitative in vitro metabolite identification in HHEP confirmed the formation of a single glucuronide conjugate of **16** (the regioselectivity was not investigated).


dx.doi.org/10.1021/jm200049r |*J. Med. Chem.* 2011, 54, 2952–2960

Interestingly, replacement of the oxetane ring in **16** by an azetidine, as in **17**, produced a compound of similar lipophilicity but with markedly reduced $CL_{int\ app}$ in HHEP (Figure 7). Mindful of this observation, we proposed that the increased human phase 2 metabolism of **16** was due to a lack of an H-bond donor or polar group at the C-5 position. This hypothesis appeared to be corroborated by the fact that *C*-aryl glucosides of similar lipophilicities, such as **18** and **19**, have a reduced $CL_{int\ app}$ (~2.0−4.0 μL/min/million cells) in HHEP. Furthermore, although relatively good potency was observed for **16**, it appeared suboptimal when compared to that of **18** ($IC_{50}$-(h-SGLT2) = 2.39 ± 1.19 nM; *n* = 6).

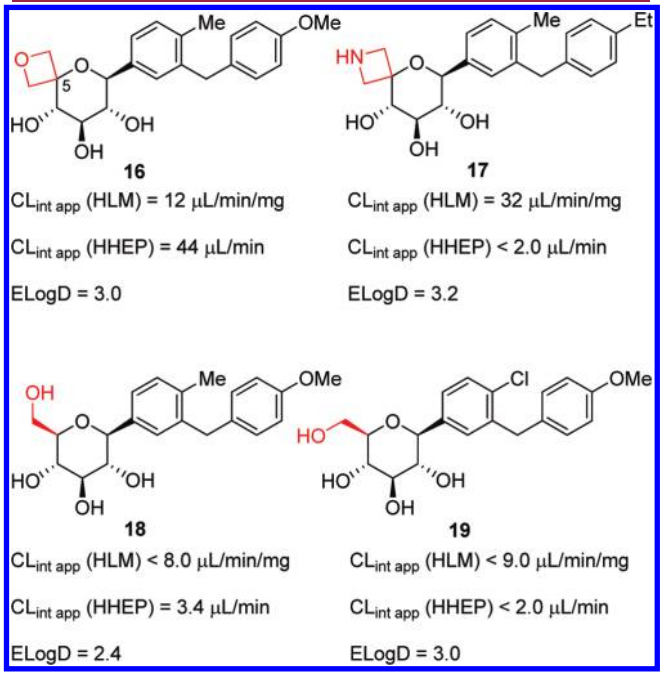


**Figure 7.** In vitro $CL_{int\ app}$ considerations. $CL_{int\ app}$(HHEP) values are expressed per million cells.

All these observations led us to deprioritize the C-5-spirocyclic *C*-glycoside SGLT2 inhibitors to focus our efforts on the dioxabicyclo[3.2.1]octane class. It was hypothesized that the bridged ketal system (Figure 2) would confer rigidity that could potentially positively impact potency and selectivity. Moreover, it would also allow introduction of a hydroxymethylene H-bond donor group (in place of the spirocycle), which was anticipated to help reduce the rate of human phase 2 metabolism (relative to that of **16**) and further improve potency.

A representative set of analogues is listed in Table 1 accompanied by in vitro data. Compounds from the class proved to be potent and very selective SGLT2 inhibitors.[42] The configuration of the stereocenter at C-4 turned out to have a profound effect on potency (~50−100-fold) with a marked preference for the *R* configuration (compare compounds **22** and **23** and compounds **4** and **24**). Interestingly, compound **20**, which bears the same diarylmethane group as **16** and has lipophilicity similar to that of **16** (as measured by ELogD),[43] demonstrated comparable $CL_{int\ app}$ in HLM but exhibited a marked decrease (>10-fold) in $CL_{int\ app}$ measured in HHEP. The reduction in HHEP $CL_{int\ app}$ to levels similar to those found in compounds **17**, **18**, and **19** was also observed for other compounds from the class (Table 1).

Upon further profiling and in vivo PK experiments in Sprague−Dawley rats, compound **4** emerged as being very promising (Table 2). It is interesting to note that, despite a low predicted clearance in HHEP, compounds **20**, **21**, and **22** displayed high clearance in the rat. It is possible that subtle species differences may exist between rats and humans with regard to oxidative and conjugative metabolism, resulting in a higher $CL_{plasma}$ in the rat in these instances. However, whereas compounds **20**−**22** showed $CL_{plasma}$ similar to that of **16**, compound **4** showed a major improvement. In particular, a marked decrease in $CL_{plasma}$ (~5-fold) and an increase in $t_{1/2}$ (~2-fold) were observed. Although low, $CL_{renal}$ [1.11 mL/min/kg > ($fu_{plasma}$)·(GFR)] was indicative of some active renal clearance. This was corroborated in vitro by the very weak uptake of **4** by rOct2 and rOat3 transporters.[44] On the other hand, there was no uptake by hOAT1, hOAT3, or hOCT2 transporters.

**Table 1. Representative Set of in Vitro Data**

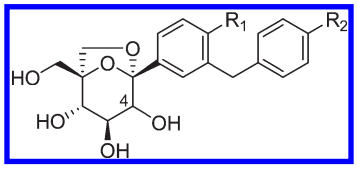


| | | | | | $fu_{plasma}$[b] | | $IC_{50}$ ± SD[c,d] (nM) | | $CL_{int\ app}$[e] | |
|---|---|---|---|---|---|---|---|---|---|---|
| compd | $R_1$ | $R_2$ | C-4[a] | ELogD | human | rat | h-SGLT2 | h-SGLTl | HLM [μL/min/mg] | HHEP [μL/min/million] |
| **20** | Me | OMe | *R* | 2.6 | 0.206 | 0.186 | 1.07 ± 0.423 (*n* = 6) | 506 ± 298 (*n* = 6) | <8.0 | <2.1 |
| **21** | Me | OEt | *R* | 3.0 | | | 1.11 ± 0.359 (*n* = 6) | 958 ± 395 (*n* = 5) | 8.9 | <2.0 |
| **22** | Cl | OMe | *R* | 3.2 | | | 0.882 ± 0.366 (*n* = 7) | 546 ± 136 (*n* = 7) | 9.2 | <2.0 |
| **23** | Cl | OMe | *S* | 3.9 | | | 43.1 ± 14.2 (*n* = 4) | >10000(*n* = 3) | 15 | 2.3 |
| **4** | Cl | OEt | *R* | 3.6 | 0.064 | 0.040 | 0.927 ± 0.369 (*n* = 10)[f] | 2050 ± 642 (*n* = 8)[g] | 12 | 4.5 |
| **24** | Cl | OEt | *S* | 3.8 | | | 89.9 ± 28.2 (*n* = 3) | >10000 (*n* = 2) | | |

[a] Configuration of the stereocenter at C-4. [b] Fraction unbound in plasma at 1000 ng/mL as measured by the equilibrium dialysis method. [c] The potency at human SGLT (h-SGLT), reported as the arithmetic mean, was evaluated using a functional assay designed to detect the inhibition of methyl α-D-glucopyranoside (AMG) uptake via the SGLT transporter expressed in CHO cells. [d] Number of runs indicated in parentheses. [e] Apparent intrinsic clearance determined by scaling $t_{1/2}$ obtained from in vitro microsome or hepatocyte incubations. [f] $IC_{50}$(h-SGLT2) = 0.877 nM (95% CI = 0.704−1.09 nM) as the geometric mean of 10 replicates. [g] $IC_{50}$(h-SGLT1) = 1960 nM (95% CI = 1460−2620 nM) as the geometric mean of eight replicates.


dx.doi.org/10.1021/jm200049r |*J. Med. Chem.* 2011, 54, 2952–2960

**Table 2. Rat IV PK Parameters**[a]

| compd | $CL_{plasma}$ (mL/min/kg) | $V_{ss}$ (L/kg) | $t_{1/2}$ (h) |
|---|---|---|---|
| **4** | 4.04 | 1.13 | 4.1 |
| **20** | 37.1 | 1.71 | 0.96 |
| **21** | 27.7 | 1.03 | 0.94 |
| **22** | 23.8 | 1.82 | 1.6 |
| **16** | 22.3 | 2.27 | 1.9 |

[a] PK experiments were conducted in male Sprague−Dawley rats ($n$ = 2 per group) at doses of 2 mg/kg (iv). iv formulation for **4**: DMSO/PEG400/30% SBECD (10/30/60, v/v/v). iv formulation for **16**, **20**, **21**, and **22**: DMA/PG/50 mM Tris base (5/10/85, v/v/v).

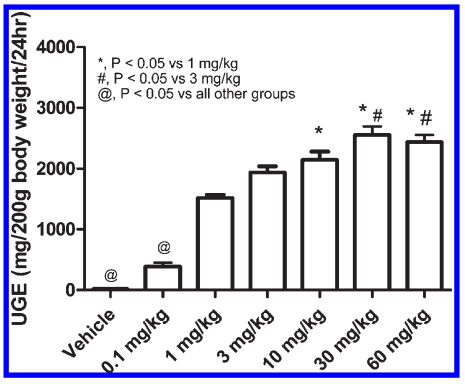


**Figure 8.** Rat 24 h UGE following treatment with **4**. Male Sprague−Dawley rats ($n$ = 5 per group) were randomized to receive one of six doses of compound **4** (0.1, 1, 3, 10, 30, and 60 mg/kg) by oral gavage. The formulation used was 20% (v/v) PEG400/24% (v/v) HPBCD. Following compound administration, urine was collected over 24 h for measurement of UGE. Simultaneously, drug exposure was assessed in satellite animals ($n$ = 2 per group).

Following 5.0 mg/kg oral administration to rats of a crystalline form of **4** (as an L-pyroglutamic acid cocrystal), the maximal systemic exposure and the time to reach peak concentrations were 1.94 ± 0.185 μg/mL and 1.0 h, respectively. The oral bioavailability ($F$) of **4** was 69%. Finally, from a safety perspective, we observed that **4** tested negative in the in vitro micronucleus test.[45]

The promising profile of **4** prompted evaluation of its potential to induce UGE in vivo. Compared to the vehicle, the compound caused a dose-responsive increase in UGE in rats for all the doses tested (Figure 8). The maximal UGE (2554 ± 141.1 mg/200 g of body weight) over 24 h was reached at a single oral dose of 30 mg/kg corresponding to a free $C_{av}$ of 408 nM (free $AUC_{0-24}$ = 4280 ng·h/mL).[46] The free in vivo $IC_{50}$ was 1.8 nM (95% CI = 1.0−2.6 nM), in good agreement with the rat SGLT2 in vitro $IC_{50}$ of 1.15 nM (95% CI = 0.757−1.74 nM; $n$ = 4).[32]

Having established the robust PD effect in rats, we then used our SGLT2 PKPD model to predict the effect of compound **4** on UGE in humans. Using allometric scaling, the predicted human $CL_{plasma}$ and $V_{ss}$ were 1.7 mL/min/kg and 1.8 L/kg, respectively. In turn, clearance and volume translated into a predicted $t_{1/2,human}$ of 12 h. As shown by the predicted steady-state dose−response curve for **4** (Figure 9), the increase of the key parameter $t_{1/2,human}$ translated into a low predicted $ED_{50}$ of 4 mg once a day at steady state in healthy volunteers to produce a 32.5 g UGE/24 h ($E_{max}$ = 65 g UGE/day).[47] The corresponding free

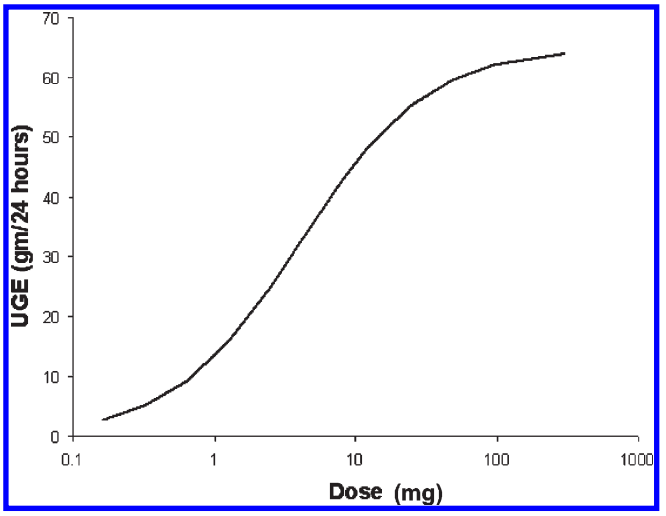


**Figure 9.** Predicted steady-state dose−response curve for **4** in healthy volunteers.

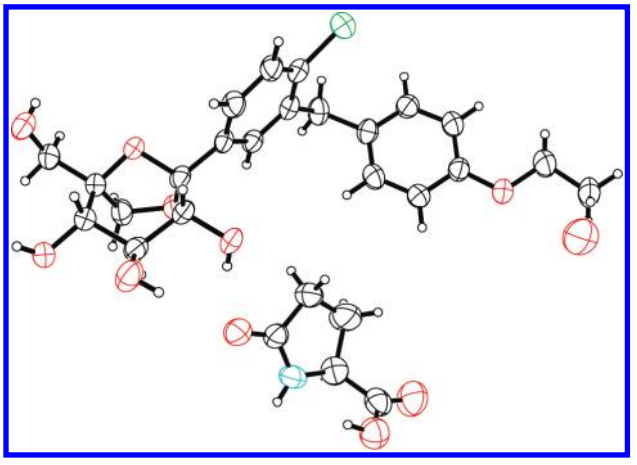

**Figure 10.** ORTEP representation of the X-ray crystal structure of a cocrystal of **4**.

in vivo $IC_{50}$ was predicted to be 1.4 nM. Using single species allometry, human $F$ was estimated to be 65% for the L-pyroglutamic acid cocrystal form of **4**.

On the basis of the excellent preclinical data package and the successful completion of regulatory toxicology studies, the compound was advanced to clinical trials as the L-pyroglutamic acid cocrystal form (mp = 142.5 °C) (Figure 10).[25] Importantly, the PKPD model proved very reliable in predicting the pharmacokinetics and pharmacological effects observed in healthy volunteers during phase 1 trials. These clinical data will be reported in due course.

## CONCLUSION

We have identified a new class of potent and selective SGLT2 inhibitors incorporating a unique dioxa-bicyclo[3.2.1]octane motif. The medicinal chemistry strategy focused on lowering of the human dose through increasing $t_{1/2}$ (via reducing the clearance) and improving the potency. This strategy was supported by (1) innovative chemistry that allowed difficult, yet very desirable, targets to be synthesized in an analogue-friendly fashion and (2) the development of a PKPD model that helped

confidently predict the human dose and reduce the discovery cycle time. Overall, these efforts supported the advancement of compound **4** into clinical development for type 2 diabetes treatment.

## EXPERIMENTAL SECTION

Unless specified otherwise, starting materials are generally available from commercial sources. NMR spectra were recorded on a Varian Unity 400 (available from Varian Inc., Palo Alto, CA) at room temperature at 400 MHz for proton. Chemical shifts are expressed in parts per million ($\delta$) relative to residual solvent as an internal reference (for methanol-*d*, $\delta$H = 3.29 ppm and $\delta$C = 47.8 ppm). The peak shapes are denoted as follows: s, singlet; d, doublet; dd, doublet of doublets; t, triplet; q, quartet; m, multiplet; br s, broad singlet; 2s, two singlets; br d, broad doublet. Electrospray (ES) ionization mass spectra were obtained on a Waters ZMD instrument (carrier gas, nitrogen; solvent A, water/0.01% formic acid; solvent B, acetonitrile/0.005% formic acid; available from Waters Corp., Milford, MA). High-resolution mass spectrometry (HRMS) was performed with an Agilent model 6210 time-of-flight instrument. Where the intensity of single chlorine ions is described, the expected intensity ratio was observed (approximately 3:1 for $^{35}Cl/^{37}Cl$-containing ions) and the intensity of only the lower mass ion is given. Column chromatography was performed with either Baker silica gel (40 $\mu$m; J.T. Baker, Phillipsburg, NJ) or silica gel 50 (EM Sciences, Gibbstown, NJ) in glass columns or in Flash 40 Biotage columns (ISC, Inc., Shelton, CT). MPLC (medium-pressure liquid chromatography) was performed using a Biotage SP purification system or a Combiflash Companion from Teledyne Isco; Biotage SNAP cartridge KPsil or Redisep Rf silica (from Teledyne Isco) under low nitrogen pressure was used. HPLC was performed using a Shimadzu 10A LC−UV or an Agilent 1100 preparatory HPLC instrument. The tested compounds were determined to be >95% pure by HPLC (see experimental details related to each tested compound for the specific conditions). Except where otherwise noted, all reactions were run under an inert atmosphere of nitrogen gas using anhydrous solvents. Also, except where otherwise noted, all reactions were run at room temperature (~23 °C).

**(2*R*,3*S*,4*S*)-2,3,4-Tris(benzyloxy)-5-hydroxy-6-[(4-methoxybenzyl)oxy]-5-[[(4-methoxybenzyl)oxy]methyl]hexanoic Acid Methoxymethylamide (5).** To a solution of **9**[25] (10.4 g, 14.5 mmol) and *N*,*O*-dimethylhydroxylamine hydrochloride (1.77 g, 29.0 mmol) in dichloromethane (100 mL) at 0 °C was added dropwise a 2.0 M solution of trimethylaluminum in hexanes (14.5 mL, 29.0 mmol), and the resulting solution was stirred at room temperature for 16 h. The reaction mixture was cooled to 0 °C and quenched by slow addition of aqueous 1 N hydrochloric acid solution. The resulting mixture was allowed to stir for 1 h. The organic phase was separated and washed with aqueous 1 N hydrochloric acid solution, dried over sodium sulfate, filtered, and concentrated under reduced pressure. The crude material was purified by medium-pressure chromatography (gradient of 5−40% ethyl acetate in heptane), yielding 6.5 g (58%) of product **5**. $^1$H NMR (400 MHz, $CDCl_3$): $\delta$ (ppm) 2.62 (br s, 1H), 2.94 (br s., 3H), 3.23 (br s, 3H), 3.42 (d, *J* = 9.4 Hz, 1H), 3.50−3.60 (m, 3H), 3.75 (s, 3H), 3.77 (s, 3H), 4.03 (d, *J* = 6.9 Hz, 1H), 4.20 (dd, *J* = 6.9, 3.3 Hz, 1H), 4.31−4.44 (m, 5H), 4.46−4.51 (m, 2H), 4.53 (d, *J* = 12 Hz, 1H), 4.66 (d, *J* = 12 Hz, 1H), 4.80 (br d, *J* = 11.5 Hz, 1H), 4.87 (d, *J* = 11.4 Hz, 1H), 6.77−6.83 (m, 4H), 7.15−7.35 (m, 19H). HRMS: *m*/*z* calcd for $C_{46}H_{54}NO_{10}$ ($M + H^+$) 780.3742, found 780.3708.

**(1*S*,2*S*,3*S*,4*R*,5*S*)-5-[4-Chloro-3-(4-ethoxybenzyl)phenyl]-1-(hydroxymethyl)-6,8-dioxa-bicyclo[3.2.1]octane-2,3,4-triol (4) and (1*S*,2*S*,3*S*,4*S*,5*S*)-5-[4-Chloro-3-(4-ethoxybenzyl)-phenyl]-1-(hydroxymethyl)-6,8-dioxa-bicyclo[3.2.1]octane-2,3,4-triol (24).** *n*-Butyllithium (1.0 mL, 2.5 M (hexanes), 3.25 equiv) was added dropwise (1 drop every 5 s) to an oxygen-degassed solution (placed in a predried Biotage microwave vial, 10−20 mL, sealed with its cap and placed under a positive stream of nitrogen gas) of 4-bromo-1-chloro-2-(4-ethoxybenzyl)benzene (815 mg, 3.25 equiv) in anhydrous tetrahydrofuran (2.9 mL) at −78 °C, and the resulting solution was stirred at this temperature for an additional hour. A solution of **5** (600 mg) in anhydrous tetrahydrofuran (1.45 mL) was then added dropwise over 1.3 h using a syringe pump, and the resulting mixture was stirred at −78 °C for 1 h before being allowed to warm to −25 °C over 14 h [put in a deep Dewar covered with aluminum foil to maintain the cold temperature (size of the Dewar: external diameter, 10 cm; internal diameter, 8 cm; height, 9 cm)]. Diethyl ether was added, and the reaction was quenched by dropwise addition of aqueous 1 M hydrochloric acid solution. The resulting biphasic mixture was stirred at room temperature for 15 min. The organic phase was separated, washed with brine, dried over magnesium sulfate, filtered, and concentrated. Chromatography over silica gel using a gradient of 10−40% ethyl acetate in heptane gave intermediate (4*S*,5*S*)-3,4,5-tris(benzyloxy)-2-[4-chloro-3-(4-ethoxybenzyl)-phenyl]-6,6-bis[[(4-methoxybenzyl)oxy]methyl]tetrahydropyran-2-ol as a mixture of isomers (280 mg, 38% yield). HRMS: *m*/*z* calcd for $C_{59}H_{61}O_{10}ClNa$ ($M + Na^+$) 987.3845, found 987.3840.

To a solution of the above intermediate (1.46 g) in dichloromethane (31 mL) was added anisole (900 $\mu$L, ~5 equiv) followed by 31 mL of a solution of 20% trifluoroacetic acid in dichloromethane, and the resulting mixture was stirred at room temperature for 1 h. The mixture was concentrated, and the crude material was chromatographed over silica gel using a gradient of 10−30% ethyl acetate in heptane to afford intermediate {(2*S*,3*S*)-2,3,4-tris(benzyloxy)-5-[4-chloro-3-(4-ethoxybenzyl)-phenyl]-6,8-dioxa-bicyclo[3.2.1]oct-1-yl}methanol as a mixture of isomers (670 mg, 63% yield). HRMS: *m*/*z* calcd for $C_{43}H_{44}O_7Cl$ ($M + H^+$) 707.2770, found 707.2765.

To a solution of the above intermediate (335 mg) in ethanol/tetrahydrofuran (10 mL; 4/1, v/v) were added successively formic acid (420 $\mu$L, 22 equiv) and palladium black (208 mg, 4 equiv), and the resulting mixture was stirred at room temperature. After 1 h, additional formic acid (420 $\mu$L, 22 equiv) and palladium black (208 mg, 4 equiv) were added, and the mixture was allowed to stir for an additional hour at room temperature. The palladium was filtered, and the crude mixture obtained after evaporation of the solvent was purified by preparative HPLC. Preparative HPLC: reversed-phase C18 Gemini column, 5 $\mu$m, 30 × 100 mm, 40 mL/min; gradient of acetonitrile/0.1% formic acid: water/0.1% formic acid, 25−50% acetonitrile/0.1% formic acid over 18 min. UV detection: 220 nm. HPLC indicated a ratio of diastereomers of 1.1:1 (**4**:**24**).

The fractions containing the product **4** were concentrated under reduced pressure. The crude material was precipitated from ethyl acetate and heptane. The resulting white solid was washed with heptane two times and dried under reduced pressure. Yield: 60 mg, 29%. $t_R$ = 12.4 min. $^1$H NMR (400 MHz, $CD_3OD$): $\delta$ (ppm) 7.43 (d, 1H, *J* = 1.9 Hz), 7.36 (dd, 1H, *J* = 8.3 and 2 Hz), 7.32 (d, 1H, *J* = 8.3 Hz), 7.08−7.04 (m, 2H), 6.79−6.75 (m, 2H), 4.12 (d, 1H, *J* = 7.5 Hz), 4.00 (s, 2H), 3.96 (q, 2H, *J* = 7.0 Hz), 3.81 (d, 1H, *J* = 12.5 Hz), 3.75 (dd, 1H, *J* = 8.3 and 1.3 Hz), 3.65 (d, 1H, *J* = 12.5 Hz), 3.63 (t, 1H, *J* = 8.2 Hz), 3.57 (dd, 1H, *J* = 7.5 and 1.3 Hz), 3.52 (d, 1H, *J* = 8.0 Hz), 1.33 (t, 3H, *J* = 6.9 Hz). $^{13}$C NMR (100 MHz, $CD_3OD$): $\delta$ (ppm) 14.0, 38.1, 60.7, 63.2, 66.7, 71.9, 76.6, 78.1, 85.0, 108.4, 114.3 (2C), 125.9, 128.6, 129.3, 129.6 (2C), 131.6, 133.8, 137.4, 138.5, 157.7. HRMS: *m*/*z* calcd for $C_{22}H_{26}O_7Cl$ ($M + H^+$) 437.1361, found 437.1360.

The fractions containing the product **24** were concentrated under reduced pressure. The crude material was precipitated from ethyl acetate and heptane. The resulting white solid was washed with heptane two times and dried under reduced pressure. Yield: 30 mg, 15%. $t_R$ = 13.2 min. $^1$H NMR (400 MHz, $CD_3OD$): $\delta$ (ppm) 7.48 (d, 1H, *J* = 1.9 Hz), 7.40 (dd, 1H, *J* = 8.1 and 1.9 Hz), 7.32 (d, 1H, *J* = 8.3 Hz), 7.08−7.03 (m, 2H), 6.80−6.74 (m, 2H), 4.04−3.99 (m, 3H), 3.95 (q, 2H, *J* = 7 Hz),

3.89−3.81 (m, 4H), 3.73 (d, 1H, $J$ = 12.5 Hz), 3.49 (d, 1H, $J$ = 7.3 Hz), 1.32 (t, 3H, $J$ = 7 Hz). HRMS: $m/z$ calcd for $C_{22}H_{26}O_7Cl$ ($M + H^+$) 437.1361, found 437.1358.

**(1*S*,2*S*,3*S*,4*R*,5*S*)-1-(Hydroxymethyl)-5-[3-(4-methoxybenzyl)-4-methylphenyl]-6,8-dioxa-bicyclo[3.2.1]octane-2,3,4-triol (20)[25].** This compound was obtained using procedures analogous to the preparation of compounds **4** and **24**. Preparative HPLC method: reversed-phase C18 Phenomenex column, Luna, 5 $\mu$m, 150 × 21.20 mm, 20 mL/min; gradient of acetonitrile/0.1% formic acid: water/0.1% formic acid, 20−60% acetonitrile/0.1% formic acid over 20 min. UV detection: 254 nm. The fractions containing the product **20** were concentrated under reduced pressure. The crude material was precipitated from ethyl acetate and heptane. The resulting white solid was washed with heptane two times and dried under reduced pressure. Yield: 55 mg, 39%. $t_R$ = 10.9 min. $^1$H NMR (400 MHz, $CD_3OD$): $\delta$ (ppm) 7.33 (d, 1H, $J$ = 1.6 Hz), 7.30 (dd, 1H, $J$ = 7.6 and 1.6 Hz), 7.10 (d, 1H, $J$ = 7.6 Hz), 7.02−6.98 (m, 2H), 6.79−6.75 (m, 2H), 4.13 (d, 1H, $J$ = 7.4 Hz), 3.90 (s, 2H), 3.82 (d, 1H, $J$ = 12.5 Hz), 3.77 (dd, 1H, $J$ = 8.2 and 1.2 Hz), 3.72 (s, 3H), 3.66 (d, 1H, $J$ = 12.5 Hz), 3.65 (t, 1H, $J$ = 8.0 Hz), 3.59 (d, 1H, $J$ = 7.8 Hz), 3.58 (dd, 1H, $J$ = 7.5 and 1.5 Hz), 2.16 (s, 3H). HRMS: $m/z$ calcd for $C_{22}H_{27}O_7$ ($M + H^+$) 403.1751, found 403.1737.

**(1*S*,2*S*,3*S*,4*R*,5*S*)-5-[3-(4-Ethoxybenzyl)-4-methylphenyl]-1-(hydroxymethyl)-6,8-dioxa-bicyclo[3.2.1]octane-2,3,4-triol (21)[25].** This compound was obtained using procedures analogous to the preparation of compounds **4** and **24**. HPLC preparative method: reversed-phase C18 Phenomenex column, Luna, 5 $\mu$m, 150 × 21.20 mm, 20 mL/min; gradient of acetonitrile/0.1% formic acid:water/0.1% formic acid, 20−60% acetonitrile/0.1% formic acid over 20 min. UV detection: 254 nm. The fractions containing the product **21** were concentrated under reduced pressure. The crude material was precipitated from ethyl acetate and heptane. The resulting white solid was washed with heptane two times and dried under reduced pressure. Yield: 20 mg, 38%. $t_R$ = 12.7 min. $^1$H NMR (400 MHz, $CD_3OD$): $\delta$ (ppm) 1.34 (t, $J$ = 6.9 Hz, 3H), 2.18 (s, 3H), 3.60 (d, $J$ = 8 Hz, 2H), 3.66 (t, $J$ = 8 Hz, 1H), 3.68 (d, $J$ = 12.5 Hz, 1H), 3.78 (d, 1H, $J$ = 8.8 Hz), 3.84 (d, $J$ = 12.4 Hz, 1H), 3.92 (s, 2H), 3.97 (q, $J$ = 7 Hz, 2H), 4.15 (d, $J$ = 7.5 Hz, 1H), 6.77 (m, 2H), 7.00 (m, 2H), 7.12 (d, $J$ = 7.7 Hz, 1H), 7.31 (dd, $J$ = 7.9 and 1.4 Hz, 1H), 7.34 (s, 1H). MS (LC−MS): $m/z$ 417.3 ($M + H^+$, positive mode), 461.4 ($M + HCO_2^-$, negative mode).

**(1*S*,2*S*,3*S*,4*R*,5*S*)-5-[4-Chloro-3-(4-methoxybenzyl)phenyl]-1-(hydroxymethyl)-6,8-dioxa-bicyclo[3.2.1]octane-2,3,4-triol (22) and (1*S*,2*S*,3*S*,4*S*,5*S*)-5-[4-Chloro-3-(4-methoxybenzyl)-phenyl]-1-(hydroxymethyl)-6,8-dioxa-bicyclo[3.2.1]octane-2,3,4-triol (23)[25].** These compounds were obtained using procedures analogous to the preparation of compounds **4** and **24**. HPLC preparative method: reversed-phase C18 Phenomenex column, Luna, 5 $\mu$m, 150 × 21.20 mm, 20 mL/min; gradient of acetonitrile/0.1% formic acid:water/0.1% formic acid, 20−60% acetonitrile/0.1% formic acid over 20 min. UV detection: 254 nm. HPLC indicated a ratio of diastereoisomers of 1.4:1 (**22**:**23**).

The fractions containing the product **22** were concentrated under reduced pressure. The crude material was precipitated from ethyl acetate and heptane. The resulting white solid was washed with heptane two times and concentrated under reduced pressure. Yield: 50 mg, 36%. $t_R$ = 12.1 min. $^1$H NMR (400 MHz, $CD_3OD$): $\delta$ (ppm) 7.43 (s, 1H), 7.38−7.30 (m, 2H), 7.08 (d, 2H), 6.79 (d, 2H), 4.12 (d, 1H, $J$ = 7.5 Hz), 4.01 (s, 2H), 3.81 (d, 1H, $J$ = 12.5 Hz), 3.75 (d, 1H, $J$ = 8.4 Hz), 3.73 (s, 3H), 3.66 (d, 1H, $J$ = 11.7 Hz), 3.63 (t, 1H, $J$ = 8.2 Hz), 3.57 (d, 1H, $J$ = 7.4 Hz), 3.52 (d, 1H, $J$ = 7.8 Hz). HRMS: $m/z$ calcd for $C_{21}H_{24}O_7Cl$ ($M + H^+$) 423.1205, found 423.1192.

The fractions containing the product **23** were concentrated under reduced pressure. The crude material was precipitated from ethyl acetate and heptane. The resulting white solid was washed with heptane two times and concentrated under reduced pressure. Yield: 37 mg, 27%. $t_R$ = 12.8 min. $^1$H NMR (400 MHz, $CD_3OD$): $\delta$ (ppm) 7.50 (d, 1H, $J$ = 1.9 Hz), 7.42 (dd, 1H, $J$ = 8.3 and 1.9 Hz), 7.35 (d, 1H, $J$ = 8.3 Hz), 7.12−7.07 (m, 2H), 6.83−6.78 (m, 2H), 4.06−4.01 (m, 3H), 3.91−3.83 (m, 4H), 3.78−3.72 (m, 4H), 3.51 (d, 1H, $J$ = 7.5 Hz). MS (LC−MS): $m/z$ 423.3 ($M + H^+$, positive mode) 467.3 ($M + HCO_2^-$, negative mode).

**4-Nitrobenzoylation of 4 To Give 14.** To a solution of **4** (10.6 mg, 0.024 mmol) in anhydrous tetrahydrofuran (300 $\mu$L) cooled at 0 °C were added *N*,*N*-diisopropylethylamine (30 $\mu$L, 7 equiv) and 4-(dimethylamino)pyridine (3 mg, 1 equiv) followed by *p*-nitrobenzoyl chloride (27 mg, 6 equiv), and the resulting mixture was stirred at 60 °C for 6 h. The mixture was cooled to room temperature, ethyl acetate and water were added, and the organic phase was successively washed with 0.5 M aqueous hydrochloric acid solution and brine. The organic phase was dried over magnesium sulfate, filtered, and concentrated, and the crude material was purified by flash chromatography over silica gel, eluting with a gradient of 10−50% ethyl acetate in heptane, to afford 18 mg of product **14** (73% yield). $^1$H NMR (400 MHz, $CDCl_3$): $\delta$ (ppm) 8.33 (m, 2H), 8.28−8.12 (m, 8H), 8.07 (m, 2H), 8.00 (m, 2H), 7.91 (m, 2H), 7.45−7.40 (m, 2H), 7.34 (d, 1H, $J$ = 8.2 Hz), 6.87 (m, 2H), 6.64 (m, 2H), 6.13 (d, 1H, $J$ = 8.6 Hz), 6.06 (t, 1H, $J$ = 8.3 Hz), 5.86 (d, 1H, $J$ = 8.1 Hz), 4.81 (d, 1H, $J$ = 8.3 Hz), 4.75 (d, 1H, $J$ = 12.7 Hz), 4.60 (d, 1H, $J$ = 12.8 Hz), 4.06 (d, 1H, $J$ = 8.5 Hz), 3.98−3.90 (m, 4H), 1.39 (t, 3H, $J$ = 7 Hz). Single crystals were obtained by slow recrystallization from acetonitrile/2-propanol as the solvent. Mp = 211 °C.

**4-Bromobenzoylation of 23 To Give 15.** To a solution of **23** (11 mg, 0.026 mmol) in anhydrous tetrahydrofuran (600 $\mu$L) were added at room temperature *N*,*N*-diisopropylethylamine (32 $\mu$L, 7 equiv) and 4-(dimethylamino)pyridine (3 mg, 0.9 equiv) followed by *p*-bromobenzoyl chloride (35 mg, 6 equiv), and the resulting mixture was stirred at room temperature for 62 h. Ethyl acetate and water were added, and the organic phase was successively washed with 0.5 M aqueous hydrochloric acid solution and brine. The organic phase was dried over magnesium sulfate, filtered, and concentrated, and the crude material was purified by flash chromatography over silica gel, eluting with a gradient of 15−30% ethyl acetate in heptane, to afford 27 mg of product **15** (90% yield). $^1$H NMR (400 MHz, $CDCl_3$): $\delta$ (ppm) 7.82 (m, 2H), 7.74−7.64 (m, 4H), 7.58−7.46 (m, 8H), 7.42−7.34 (m, 4H), 7.29 (d, 1H, $J$ = 8.3 Hz), 6.89 (m, 2H), 6.63 (m, 2H), 6.04 (dd, 1H, $J$ = 9.6 and 1 Hz), 5.98 (dd, 1H, $J$ = 9.6 and 4.4 Hz), 5.89 (d, 1H, $J$ = 4.4 Hz), 4.70 (d, 1H, $J$ = 12.4 Hz), 4.65 (d, 1H, $J$ = 12.4 Hz), 4.60 (d, 1H, $J$ = 8 Hz), 3.98−3.88 (m, 3H), 3.73 (s, 3H). Single crystals were obtained by vapor diffusion techniques using heptane and ethyl acetate as solvents. Mp = 191 °C.

## ■ ASSOCIATED CONTENT

**Supporting Information.** X-ray crystallographic data for **14**, **15**, and an L-pyroglutamic acid cocrystal form of **4** and additional discussion around the PKPD model. This material is available free of charge via the Internet at http://pubs.acs.org.

## ■ AUTHOR INFORMATION

### Corresponding Author

*Phone: (860) 686-3455. Fax: (860) 715-0310. E-mail: vincent.mascitti@pfizer.com.

## ■ ACKNOWLEDGMENT

We thank Paul DaSilva-Jardine, David Price, David Hepworth, Margaret Chu-Moyer, Spiros Liras, Roger Ruggeri, Neeta Amin, and Gianluca Nucci from Pfizer Global Research & Development for stimulating discussions.

## ■ ABBREVIATIONS USED

SGLT, sodium-dependent glucose cotransporter; UGE, urinary glucose excretion; PK, pharmacokinetics; PD, pharmacodynamics; $CL_{plasma}$, total plasma clearance; $V_{ss}$, steady-state volume of distribution; $CL_{int\ app}$, in vitro apparent intrinsic clearance; HLM, human liver microsome; HHEP, human hepatocyte; fu, fraction unbound; SD, standard deviation; GFR, glomerular filtration rate; $F$, oral bioavailability; $C_{av}$, average plasma concentration; AUC, area under the plasma concentration time curve; PEG, polyethylene glycol; PG, propylene glycol; SBECD, (sulfobutyl ester)-$\beta$-cyclodextrin; DMA, dimethylaniline; HPBCD, (hydroxypropyl)-$\beta$-cyclodextrin; $IC_{50}$, half-maximal inhibitory concentration; $ED_{50}$, half-maximal effective dose; $E_{max}$, maximum effect; CI, confidence interval; [MPG], mean plasma glucose concentration; $t_R$, retention time.

## ■ REFERENCES


(1) International Diabetes Federation. *Diabetes Atlas*, 4th ed.; International Diabetes Federation: Brussels, Belgium, 2009.

(2) (a) Levetan, C. Oral antidiabetic agents in type 2 diabetes. *Curr. Med. Res. Opin.* **2007**, *23*, 945–952. (b) Phung, O. J.; Scholle, J. M.; Talwar, M.; Coleman, C. I. Effect of noninsulin antidiabetic drugs added to metformin therapy on glycemic control, weight gain, and hypoglycemia in type 2 diabetes. *JAMA, J. Am. Med. Assoc.* **2010**, *303*, 1410–1418. (c) Pozzilli, P.; Leslie, R. D.; Chan, J.; De Fronzo, R.; Monnier, L.; Raz, I.; Del Prato, S. The A1C and ABCD of glycaemia management in type 2 diabetes: a physician's personalized approach. *Diabetes/Metab. Res. Rev.* **2010**, *26*, 239–244. (d) Laliberte, B. K.; Neumiller, J. J. Review of medications used in the treatment of diabetes mellitus. *J. Pharm. Technol.* **2010**, *26*, 136–146.

(3) Kanai, Y.; Lee, W. S.; You, G.; Brown, D.; Hediger, M. A. The human kidney low affinity $Na^+$/glucose cotransporter SGLT2. Delineation of the major renal reabsorptive mechanism for D-glucose. *J. Clin. Invest.* **1994**, *93*, 397–404.

(4) Albertoni Borghese, M. F.; Majowicz, M. P. Inhibitors of sodium/glucose cotransporter. *Drugs Future* **2009**, *34*, 297–305.

(5) Lee, W. S.; Kanai, Y.; Wells, R. G.; Hediger, M. A. The high affinity $Na^+$/glucose cotransporter. *J. Biol. Chem.* **1994**, *269*, 12032–12039.

(6) Neumiller, J. J.; White, J. R., Jr.; Campbell, R. K. Sodium-glucose co-transport inhibitors. Progress and therapeutic potential in type 2 diabetes mellitus. *Drugs* **2010**, *70*, 377–385.

(7) Chao, E. C.; Henry, R. R. SGLT2 inhibition—a novel strategy for diabetes treatment. *Nat. Rev. Drug Discovery* **2010**, *9*, 551–559.

(8) DeFronzo, R. A. From the triumvirate to the ominous octet: a new paradigm for the treatment of type 2 diabetes mellitus. *Diabetes* **2009**, *58*, 773–795.

(9) Nair, S.; Wilding, J. P. H. Sodium glucose cotransporter 2 inhibitors as a new treatment for diabetes mellitus. *J. Clin. Endocrinol. Metab.* **2010**, *95*, 34–42.

(10) For a discussion around a pathophysiologic-based algorithm for the treatment of type 2 diabetes, see ref 8.

(11) Ehrenkranz, J. R. L.; Lewis, N. G.; Kahn, C. R.; Roth, J. Phlorizin: a review. *Diabetes/Metab. Res. Rev.* **2005**, *21*, 31–38.

(12) White, J. R., Jr. Apple trees to sodium glucose co-transporter inhibitors: a review of SGLT2 inhibition. *Clin. Diabetes* **2010**, *28*, 5–10.

(13) (a) Hussey, E. K.; Clark, R. V.; Amin, D. M.; Kipnes, M. S.; O'Connor-Semmes, R. L.; O'Driscoll, E. C.; Leong, J.; Murray, S. C.; Dobbins, R. L.; Layko, D.; Nunez, D. J. R. Single-dose pharmacokinetics and pharmacodynamics of sergliflozin etabonate, a novel inhibitor of glucose reabsorption, in healthy volunteers and patients with type 2 diabetes mellitus. *J. Clin. Pharmacol.* **2010**, *50*, 623–635. (b) Hussey, E. K.; Dobbins, R. L.; Stoltz, R. R.; Stockman, N. L.; O'Connor-Semmes, R. L.; Kapur, A.; Murray, S. C.; Layko, D.; Nunez, D. J. R. Multiple-dose pharmacokinetics and pharmacodynamics of sergliflozin etabonate, a novel inhibitor of glucose reabsorption, in healthy overweight and obese subjects: a randomized double-blind study. *J. Clin. Pharmacol.* **2010**, *50*, 636–646. (c) Washburn, W. N. Development of the renal glucose reabsorption inhibitors: a new mechanism for the pharmacotherapy of diabetes mellitus type 2. *J. Med. Chem.* **2009**, *52*, 1785–1794.

(14) Meng, W.; Ellsworth, B. A.; Nirschl, A. A.; McCann, P. J.; Patel, M.; Girotra, R. N.; Wu, G.; Sher, P. M.; Morrison, E. P.; Biller, S. A.; Zahler, R.; Deshpande, P. P.; Pullockaran, A.; Hagan, D. L.; Morgan, N.; Taylor, J. R.; Obermeier, M. T.; Humphreys, W. G.; Khanna, A.; Discenza, L.; Robertson, J. G.; Wang, A.; Han, S.; Wetterau, J. R.; Janovitz, E. B.; Flint, O. P.; Whaley, J. M.; Washburn, W. N. Discovery of dapagliflozin: a potent, selective renal sodium-dependent glucose cotransporter 2 (SGLT2) inhibitor for the treatment of type 2 diabetes. *J. Med. Chem.* **2008**, *51*, 1145–1149.

(15) Washburn, W. N. Evolution of sodium glucose co-transporter 2 inhibitors as anti-diabetic agents. *Expert Opin. Ther. Pat.* **2009**, *19*, 1485–1499.

(16) (a) Nomura, S.; Sakamaki, S.; Hongu, M.; Kawanishi, E.; Koga, Y.; Sakamoto, T.; Yamamoto, Y.; Ueta, K.; Kimata, H.; Nakayama, K.; Tsuda-Tsukimoto, M. Discovery of canagliflozin, a novel *C*-glucoside with thiophene ring, as sodium-dependent glucose co-transporter 2 inhibitor for the treatment of type 2 diabetes mellitus. *J. Med. Chem.* **2010**, *53*, 6355–6360. (b) Nomura, S.; Kawanishi, E. Process for the crystalline preparation of 1-($\beta$-D-glucopyranosyl)-4-methyl-3-[5-(4-fluorophenyl)-2-thienylmethyl] benzene hemihydrate. PCT Int. Appl. WO2008069327, 2008; *Chem. Abstr.* **2008**, *149*, 32515.

(17) Imamura, M.; Murakami, T.; Shiraki, R.; Ikegai, K.; Sugane, T.; Iwasaki, F.; Kurosaki, E.; Tomiyama, H.; Noda, A.; Kitta, K.; Kobayashi, Y. Preparation of C-glycoside derivatives and salts thereof as $Na^+$-glucose co-transporter inhibitor. PCT Int. Appl. WO2004080990, 2004; *Chem. Abstr.* **2004**, *141*, 296242.

(18) (a) Eckhardt, M.; Eickelmann, P.; Himmelsbach, F.; Barsoumian, E. L.; Thomas, L. Preparation of glucopyranosyl-substituted phenyl derivatives antidiabetic agents and SGLT2 inhibitors. U.S. Patent US 7,579,449, 2009; *Chem. Abstr.* **2005**, *143*, 286629. (b) Himmelsbach, F.; Schmid, S.; Schuehle, M.; Martin, H.-J.; Eckhardt, M. Crystalline form of 1-chloro-4-($\beta$-D-glucopyranos-1-yl)-2-[4-((S)-tetrahydrofuran-3-yloxy)-benzyl]-benzene, a method for its preparation and the use thereof for preparing medicaments. U.S. Patent Appl. US 20100099641, 2010; *Chem. Abstr.* **2010**, *152*, 485704.

(19) (a) Goodwin, N. C.; Harrison, B. A.; Iimura, S.; Mabon, R.; Song, Q.; Wu, W.; Yan, J.; Zhang, H.; Zhao, M. M. Preparation of glycosyl sulfoxides as potential antidiabetic sodium glucose co-transporter 2 inhibitors. PCT Int. Appl. WO2009014970, 2009; *Chem. Abstr.* **2009**, *150*, 144780. (b) Goodwin, N. C.; Mabon, R.; Harrison, B. A.; Shadoan, M. K.; Almstead, Z. Y.; Xie, Y.; Healy, J.; Buhring, L. M.; DaCosta, C. M.; Bardenhagen, J.; Mseeh, F.; Liu, Q.; Nouraldeen, A.; Wilson, A. G. E.; Kimball, S. D.; Powell, D. R.; Rawlins, D. B. Novel L-xylose derivatives as selective sodium-dependent glucose cotransporter 2 (SGLT2) inhibitors for the treatment of type 2 diabetes. *J. Med. Chem.* **2009**, *52*, 6201–6204.

(20) Liou, J.; Wu, Y.; Li, S.; Xu, G. Processes for the preparation of C-aryl glycoside amino acid complexes as potential SGLT2 inhibitors. PCT Int. Appl. WO2010022313, 2010; *Chem. Abstr.* **2010**, *152*, 287663.

(21) Kakinuma, H.; Oi, T.; Hashimoto-Tsuchiya, Y.; Arai, M.; Kawakita, Y.; Fukasawa, Y.; Iida, I.; Hagima, N.; Takeuchi, H.; Chino, Y.; Asami, J.; Okumura-Kitajima, L.; Io, F.; Yamamoto, D.; Miyata, N.; Takahashi, T.; Uchida, S.; Yamamoto, K. (1*S*)-1,5-Anhydro-1-[5-(4-ethoxybenzyl)-2-methoxy-4-methylphenyl]-1-thio-D-glucitol (TS-071) is a potent, selective sodium-dependent glucose cotransporter 2 (SGLT2) inhibitor for type 2 diabetes treatment. *J. Med. Chem.* **2010**, *53*, 3247–3261.

(22) For a recent disclosure related to tofogliflozin, see: Sato, T.; et al. Discovery of *O*-spiroketal *C*-arylglucosides as novel and selective sodium-dependent glucose cotransporter 2 (SGLT2) inhibitor for the treatment of type 2 diabetes. *Abstracts of Papers*, 240th National ACS Meeting, Boston, MA, Aug 22−26, 2010; American Chemical Society: Washington, DC, 2010; MEDI-202.

(23) (a) Kalgutkar, A. S.; Gardner, I.; Obach, R. S.; Shaffer, C. L.; Callegari, E.; Henne, K. R.; Mutlib, A. E.; Dalvie, D. K.; Lee, J. S.; Nakai, Y.; O'Donnell, J. P.; Boer, J.; Harriman, S. P. A comprehensive listing of bioactivation pathways of organic functional groups. *Curr. Drug Metab.* **2005**, *6*, 161–225. (b) Kalgutkar, A. S.; Soglia, J. R. Minimising the potential for metabolic activation in drug discovery. *Expert Opin. Drug Metab. Toxicol.* **2005**, *1*, 91–142.

(24) Washburn, W.; Meng, W. C-aryl glucoside SGLT2 inhibitors and method for the treatment of diabetes and related diseases. U.S. Patent US 7,589,193, 2009; *Chem. Abstr.* **2006**, *144*, 305154.

(25) Mascitti, V.; Collman, B. M. Preparation of dioxa-bicyclo-[3.2.1]octane-2,3,4-triol derivatives as antidiabetic agents. PCT Int. Appl. WO2010023594, 2010; *Chem. Abstr.* **2010**, *152*, 311862.

(26) For the first disclosure of the structure of **4** and a preliminary communication of part of this work, see: Mascitti, V. Discovery of a new class of SGLT2 inhibitors. *Abstracts of Papers*, 240th National ACS Meeting, Boston, MA, Aug 22−26, 2010; American Chemical Society: Washington, DC, 2010; MEDI-21.

(27) See ref 25. See also: Gent, P. A.; Gigg, R. The allyl ether as a protecting group in carbohydrate chemistry. Part VI. The allyl ether as a "temporary" protecting group in oligosaccharide synthesis. *J. Chem. Soc., Perkin Trans. 1* **1974**, 1835–1839.

(28) Schaffer, R. Branched-chain higher sugars. III. A 4-C-(hydroxymethy1)-pentose. *J. Am. Chem. Soc.* **1959**, *81*, 5452–5454.

(29) Upon storage at room temperature for an extended period of time, we observed that **5** cyclized back to lactone **9**.

(30) The addition of anisole avoids the formation of side products arising from Friedel−Crafts-type reactions between the PMB cation and the aryl ring of the substrate.

(31) Mascitti, V.; Préville, C. Stereoselective synthesis of a dioxa-bicyclo[3.2.1]octane SGLT2 inhibitor. *Org. Lett.* **2010**, *12*, 2940–2943.

(32) For a more detailed discussion around the SGLT2 PKPD model, see the Supporting Information.

(33) Hosea, N. A.; Collard, W. T.; Cole, S.; Maurer, T. S.; Fang, R. X.; Jones, H.; Kakar, S. M.; Nakai, Y.; Smith, B. J.; Webster, R.; Beaumont, K. Prediction of human pharmacokinetics from preclinical information: comparative accuracy of quantitative prediction approaches. *J. Clin. Pharmacol.* **2009**, *49*, 513–533.

(34) This model assumes rapid drug equilibrium (plasma/urine), simple direct inhibition, and plasma glucose concentration similar to the measured fasting plasma glucose concentration. See the Supporting Information for more details.

(35) Mascitti, V.; Robinson, R. P.; Préville, C.; Thuma, B. A.; Carr, C. L.; Reese, M. R.; Maguire, R. J.; Leininger, M. T.; Lowe, A.; Steppan, C. M. Syntheses of C-5-spirocyclic *C*-glycoside SGLT2 inhibitors. *Tetrahedron Lett.* **2010**, *51*, 1880–1883.

(36) Potency at human SGLT (h-SGLT) was evaluated using a functional assay designed to detect the inhibition of methyl α-D-glucopyranoside (AMG) uptake via the SGLT transporter expressed in Chinese hamster ovary cells. See the Supporting Information for more details. For **16**, $IC_{50}$(h-SGLT2) = 6.55 nM (95% CI = 4.69−9.15 nM) as the geometric mean of eight replicates and $IC_{50}$(h-SGLT1) = 1540 nM (95% CI = 1390−1700 nM) as the geometric mean of seven replicates.

(37) Robinson, R. P.; Mascitti, V.; Boustany-Kari, C. M.; Carr, C. L.; Foley, P. M.; Kimoto, E.; Leininger, M. T.; Lowe, A.; Klenotic, M. K.; MacDonald, J. I.; Maguire, R. J.; Masterson, V. M.; Maurer, T. S.; Miao, Z.; Patel, J. D.; Préville, C.; Reese, M. R.; She, L.; Steppan, C. M.; Thuma, B. A.; Zhu, T. C-Aryl glycoside inhibitors of SGLT2: exploration of sugar modifications including C-5 spirocyclization. *Bioorg. Med. Chem. Lett.* **2010**, *20*, 1569–1572.

(38) In addition to the difficulty in rationally designing and building a structure−activity relationship around $V_{ss}$, attempts to increase $V_{ss}$ were not pursued due to the relative insensitivity of the dose to changes in this parameter.

(39) Total clearance is the sum of the hepatic clearance ($CL_{hepatic}$), renal clearance ($CL_{renal}$), and biliary clearance ($CL_{biliary}$). In first approximation the $CL_{biliary}$ component was neglected.

(40) Obtained by scaling $t_{1/2}$ derived from in vitro human microsome incubations.

(41) Obtained by scaling $t_{1/2}$ derived from in vitro human hepatocyte incubations (0.5 million cells).

(42) Compound **4** is also highly selective (>60000-fold) for SGLT2 over the facilitative glucose transporters (GLUT 1−4) on the basis of in vitro assays.

(43) For a discussion around ELogD for lipophilicity determination, see: Lombardo, F.; Shalaeva, M. Y.; Tupper, K. A.; Gao, F. ElogDoct: a tool for lipophilicity determination in drug discovery. 2. Basic and neutral compounds. *J. Med. Chem.* **2001**, *44*, 2490–2497.

(44) The in vitro transport assay used human embryonic kidney 293 cells (HEK293) transfected with the appropriate organic anion or cation transporter.

(45) Test No. 487: In Vitro Mammalian Cell Micronucleus Test. *OECD Guidelines for the Testing of Chemicals, Section 4: Health Effects*; Organisation for Economic Co-operation and Development: Paris, 2010; http://www.oecd.org/env/testguidelines. Compound **4** acts as neither an aneugen nor a clastogen in the micronucleus assay.

(46) The vehicle group resulted in a UGE over 24 h of 16.4 ± 4.69 mg/200 g of body weight.

(47) Assuming a theoretical body weight of 70 kg and [MPG] = 80 mg/dL. See the Supporting Information for more details.